Letter

# Designing robust trajectories by lobe dynamics in low-dimensional Hamiltonian systems

Naoki Hiraiwa,[1,2] Mai Bando,[1] Isaia Nisoli,[3] and Yuzuru Sato[4,5,*]

[1]*Department of Aeronautics and Astronautics, Kyushu University, 744 Motooka, Nishi-ku, Fukuoka 21941-909, Japan*

[2]*Colorado Center for Astrodynamics Research, University of Colorado Boulder, 3775 Discovery Drive, Boulder, Colorado 80303, USA*

[3]*Instituto de Matemática, Universidade Federal do Rio de Janeiro, Avenida Athos da Silveira Ramos, 149, Edifício do Centro de Tecnologia, Bloco C (Térreo), Cidade Universitária 8190395, Brazil*

[4]*RIES-MSC/Department of Mathematics, Hokkaido University, N12 W7 Kita-ku, Sapporo, Hokkaido 0600812, Japan*

[5]*London Mathematical Laboratory, 14 Buckingham Street, London WC2N 6DF, United Kingdom*

(Received 10 January 2024; accepted 1 April 2024; published 24 May 2024)

Modern space missions with uncrewed spacecraft require robust trajectory design to connect multiple chaotic orbits by small controls. To address this issue, we propose a control scheme to design robust trajectories by leveraging a geometrical structure in chaotic zones, known as a *lobe*. Our scheme shows that appropriately selected lobes reveal possible paths to traverse chaotic zones in a short time. The effectiveness of our method is demonstrated through trajectory design in both the standard map and Hill's equation.

DOI: 10.1103/PhysRevResearch.6.L022046

The Artemis program [1], including the uncrewed cargo mission to the lunar Gateway [2], has attracted significant attention from aerospace engineers. This mission demands frequent transportation from the Earth to the lunar Gateway, emphasizing the need for a method to design a robust transfer. Additionally, many recent deep-space missions aimed at enhancing our knowledge of planetary science [3] have utilized small satellites with limited fuel and maneuver capabilities. In such modern space missions with uncrewed spacecraft, trajectory design must incorporate chaotic orbits because spacecraft are expected to traverse chaotic zones to reach the Moon under severe thrust and transfer time conditions. To address these issues, we propose a control scheme to design robust trajectories by leveraging a geometrical structure in chaotic zones, known as a *lobe* [4].

Conventionally, spacecraft trajectories affected by the gravity of celestial bodies have been designed by connecting paths near tori in Hamiltonian systems with adequate controls. In the two-body problem, optimal trajectories are formed based on Hohmann transfer—the minimum-fuel two-impulsive transfer between coplanar circular orbits, or flyby, which is a gravity-assist maneuver by a planet [5]. For the restricted three-body problems, several effective techniques have been studied, including *tube dynamics*, which constitutes the transport structure of cylindrical invariant manifolds [6,7], ballistic lunar transfers, which efficiently utilize solar forces [8,9], and resonant gravity assist, which consists of multiple flybys around the same planet [10].

The primary obstacle in trajectory design is to handle chaotic orbits. In the literature on nonlinear dynamics, the concept of controlling chaos [11,12] focuses on stabilizing chaotic motion through small perturbations to the system. Conversely, harnessing chaos [13,14] attempts to exploit the characteristics of chaotic motion, including so-called *targeting* [15], where the sensitivity to initial conditions is used to swiftly direct the system to a desired point in state space. The trajectory design in the Earth-Moon system has been studied following the seminal work by Bollt and Meiss [16], which introduced an approach to shorten a natural chaotic transfer trajectory by leveraging recurrence and instability. Subsequently, Schroer and Ott developed the pass targeting method [17]. Another research direction involves trajectory design based on Lagrangian coherent structures. This line of research focuses on adding small controls to get over a separatrix between different coherent structures in fluid dynamics [18–21]. These methods are similar to the control techniques based on tube dynamics in spacecraft trajectory design [6].

In this Letter, we present a control method to design robust trajectories based on lobe dynamics, which is a finer geometrical structure than tube dynamics. Although lobe dynamics has been studied to analyze transport in dynamical systems [22–26], it has not been used for trajectory design. We establish a framework to design robust trajectories to connect start and goal orbits via a few chaotic orbits within selected lobes. As a result, we notably find shorter-time transfers than those in the previous work in the Earth-Moon system [16,17].

To design finite-time trajectories in Hamiltonian systems, we presume knowledge regarding the equation of motion and the instant measurements of the spacecraft's position and velocity. Moreover, we assume that the trajectories remain in the same energy surface in a Hamiltonian system before and after control. Our investigation is focused on a specific finite-time trajectory, departing from a start orbit in an elliptic

[*]ysato@math.sci.hokudai.ac.jp

island and arriving at a goal orbit in another elliptic island in a low-dimensional Hamiltonian system.

We illustrate our scheme in the standard map and Hill's equation. The former demonstrates a simple example for our method, while the latter applies it to a more realistic scenario. The standard map [27] serves as the simplest model of Hamiltonian systems, expressed as

$$\begin{aligned} p_{n+1} &= p_n + K \sin\theta_n, \\ \theta_{n+1} &= \theta_n + p_{n+1} \pmod{2\pi}, \end{aligned} \tag{1}$$

where the Hamiltonian of the flow is given as $H(p,\theta,t) = p^2/2 + K\cos\theta \sum_{n=-\infty}^{\infty} \delta(t-n)$. We set $K = 1.2$ as an example, which gives nonintegrable chaotic dynamics for many orbits with a positive top Lyapunov exponent. Hill's equation [28] is a nondimensional model for the Earth-Moon planar circular restricted three-body problem, expressed as

$$\begin{aligned} \ddot{x} - 2\dot{y} - x &= -\frac{(1-\mu)(x+\mu)}{{r_1}^3} - \frac{\mu(x-1+\mu)}{{r_2}^3}, \\ \ddot{y} + 2\dot{x} - y &= -\frac{(1-\mu)y}{{r_1}^3} - \frac{\mu y}{{r_2}^3}, \end{aligned} \tag{2}$$

where the position of a spacecraft is $(x, y)$, $r_1 = \sqrt{(x+\mu)^2 + y^2}$, $r_2 = \sqrt{(x-1+\mu)^2 + y^2}$, and the masses for the Earth and Moon are given as $1-\mu$ and $\mu$, respectively. In these standard coordinates, the unit of length is the distance between the Earth and Moon given as $3.844 \times 10^5$ (km), the unit of mass is the sum of the masses of the Earth and Moon as $6.046 \times 10^{24}$ (kg), and the unit of time is the inverse of the rotation rate in the system as 1.042 (h). The Jacobi integral given by

$$J = x^2 + y^2 + 2\frac{1-\mu}{r_1} + 2\frac{\mu}{r_2} + \mu(1-\mu) - (\dot{x}^2 + \dot{y}^2)$$

restricts the flow to a three-dimensional subspace in the four-dimensional state space. We set $\mu = 1.215\,09 \times 10^{-2}$ and $J = 3.16$, which possesses a sufficient energy level to enable transfers from the Earth to the Moon and indicates chaotic dynamics.

The key concept in our control scheme is lobe dynamics [4], which was initially conceptualized for analyzing phase space volume transportation in Hamiltonian systems [29]. The lobes are identified by finding two hyperbolic periodic points, $p_1$ and $p_2$, within the two-dimensional state space of an area- and orientation-preserving map $F$. In chaotic systems, the stable and unstable manifolds of $p_1$ and $p_2$ can intersect infinitely many times if they lie in the same chaotic zone. By identifying two adjacent intersection points, $q_0$ and $q_1$, the region enclosed by segments of the stable and unstable manifolds between these points constitutes a lobe [4]. A *lobe sequence* is defined as a series of lobes mapped by $F$. Each pair of stable/unstable manifolds may form multiple lobe sequences. Figure 1 schematically illustrates two such sequences originating from $L_1$ and $L_2$, mapped by $F$. Because one lobe is mapped to another by $F$, the trajectories starting within the same lobe exhibit similar behavior over a finite time and are encircled by invariant manifolds associated with unstable periodic points. This characteristic makes lobes suitable for robust trajectory design in our scheme. However, lobes, being infinite in number, eventually fold intricately to become dense

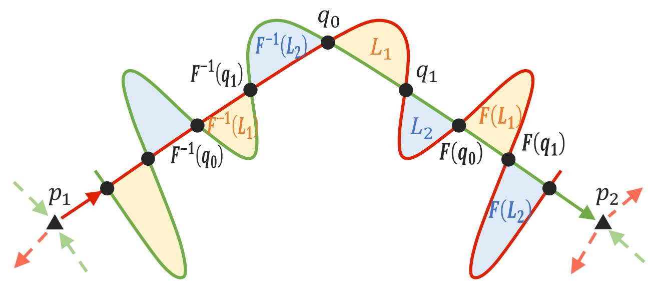


FIG. 1. Lobes $L_1, L_2$, and their transport by an area- and orientation-preserving map $F$. Hyperbolic periodic points, $p_1$ and $p_2$, and intersection points are denoted as triangles and black dots, respectively. The stable and unstable manifolds associated with the periodic points are depicted by green and red lines, respectively. Yellow and blue regions represent two different lobe sequences.

in the chaotic zone. To leverage lobe sequences for robust trajectory design, we provide the definition of an *effective lobe sequence*. Let $B_\varepsilon(c)$ be $\varepsilon$-ball with the center $c$ in a lobe. The radius $r_L$ of a lobe $L$ is defined as the largest $\varepsilon$ in all possible $B_\varepsilon(c)$'s in the lobe; $r_L := \max_{c\in L, B_\varepsilon(c)\subset L} \varepsilon$. As the mapping iterates, lobes are typically stretching out with a positive Lyapunov exponent, and the sequence of the radii of the lobes asymptotically converges to 0. Therefore, an effective lobe sequence is defined as a lobe sequence composed of a finite number of the lobes whose radius is larger than a minimum lobe radius $r^*$. For practical computations, the radius $r_L$ is estimated as the Hausdorff semidistance between the lobe's center of gravity and its boundary. This radius indicates allowable observational/operational error bounds during a transfer.

Figure 2 outlines our control scheme, which establishes a start point on the start orbit $O_s$ and a goal point on the goal orbit $O_g$ to construct the desired orbit-to-orbit transfer with the smallest total control cost. The definition of control costs depends on application. Given a trajectory connecting $O_s$, effective lobe sequences $S_i$ $(i = 1, 2, \ldots, N-1)$, and $O_g$

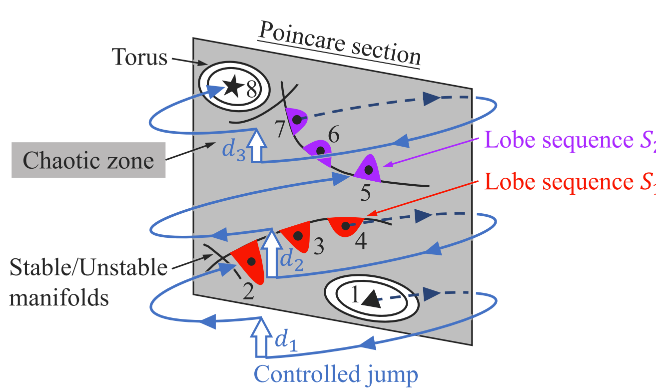


FIG. 2. Schematic view of our control. The start point, goal point, and centers of gravity of the lobes are denoted as a triangle, a star, and black dots, respectively. Finitely long effective lobe sequences $S_i$ $(i = 1, 2)$ are used for the transfer. In this example, three controlled jumps outside the Poincaré section are required to connect two orbits in different elliptic islands. The numbers indicate the order of the transfer. The total control cost $D = \sum_{k=1}^{N} d_k$ $(N = 3$ here) is minimized.

by external controls, this trajectory becomes a robust transfer bounded by the segments of stable and unstable manifolds. In our scheme, this designed trajectory first jumps from a start point on $O_s$ to a point on $S_1$ at a control cost $d_1$. The trajectory remains within $S_1$ without control before the next jump to $S_2$ at a cost $d_2$. Controlled jumps from $S_i$ to $S_{i+1}$ are repeated until the trajectory reaches $O_g$ by the $N$th jump at a cost $d_N$. These controlled jumps between lobe sequences help overcome the partial barriers formed by the boundaries of resonances [30,31] or cantori [32]. Although the trajectory may remain within the same lobe sequence for an extended period without control, it is necessary to jump to another effective lobe sequence within a finite time for maintaining system controllability, because the radius of a lobe eventually converges to zero. Thus, a small number of the selected lobe sequences contribute to short-time transfers. The control costs $\{d_k\}$ are determined under the following constraints:

(1) The trajectory moves to the center of gravity of an effective lobe with $r_L > r^*$ or a goal point on $O_g$ by control.

(2) The cost of each jump $d_k$ satisfies $0 < d_k < d^*$.

(3) The trajectory remains within an effective lobe sequence for at least one step.

(4) Minimize the total cost $D = \sum_{k=1}^{N} d_k$.

The maximum control cost $d^*$ represents the maximum thrust of the engines at one step. Before optimization, we predetermine potential start points on $O_s$, potential goal points on $O_g$, and the constraint parameters $r^*$ and $d^*$. To select effective lobe sequences, we first select candidates for the first effective lobe sequence $S_1$ that can be reached from the potential start points on $O_s$ by a controlled jump with $d_1 < d^*$. Similarly, we then explore candidates for $S_2$ reachable from $S_1$. This procedure concludes with finding candidates for the final effective lobe sequence accessible to the goal points on $O_g$ by a controlled jump with $d_N < d^*$. For any pair of $O_s$ and $O_g$ in different elliptic islands, if there exists a chaotic zone between them, we can find lobe sequences by using a sufficiently small $r^*$ and sufficiently large $d^*$ given that a lobe sequence can approach any elliptic islands in the long run. The optimization is performed for finite combinations of jumps among the start points, a few effective lobe sequences, and the goal points. A larger $r^*$ and smaller $d^*$ contribute to reducing the computational cost for the optimization. A detailed explanation of this optimization is presented in the Supplemental Material [33].

We first apply our control scheme to the standard map, given by the stroboscopic map of the kicked rotator. Starting with $(p_n, \theta_n)$ on the Poincaré section at time $t = n$, the momentum changes to $p_n + K \sin\theta_n$, and then is adjusted to $p_n + K \sin\theta_n + \Delta p_n$ by a control at time $t = n + \eta_n$ $(0 < \eta_n < 1)$. The position $\theta_n$ is integrated with the modified momentum after $t = n + \eta_n$. Upon returning to the Poincaré section at time $t = n + 1$, the controlled jump to $(p'_{n+1}, \theta'_{n+1})$ is established as

$$\begin{aligned} p'_{n+1} &= p_n + K \sin\theta_n + \Delta p_n = p_{n+1} + \Delta p_n, \\ \theta'_{n+1} &= \theta_n + p_{n+1} + (1 - \eta_n)\Delta p_n \\ &= \theta_{n+1} + (1 - \eta_n)\Delta p_n. \end{aligned} \tag{3}$$

Because the combinations of $(p_n, \theta_n)$ and $(p'_{n+1}, \theta'_{n+1})$ are given in the optimization process, we can compute the control parameters $\Delta p_n$ and $\eta_n$ from Eq. (3). Within this control

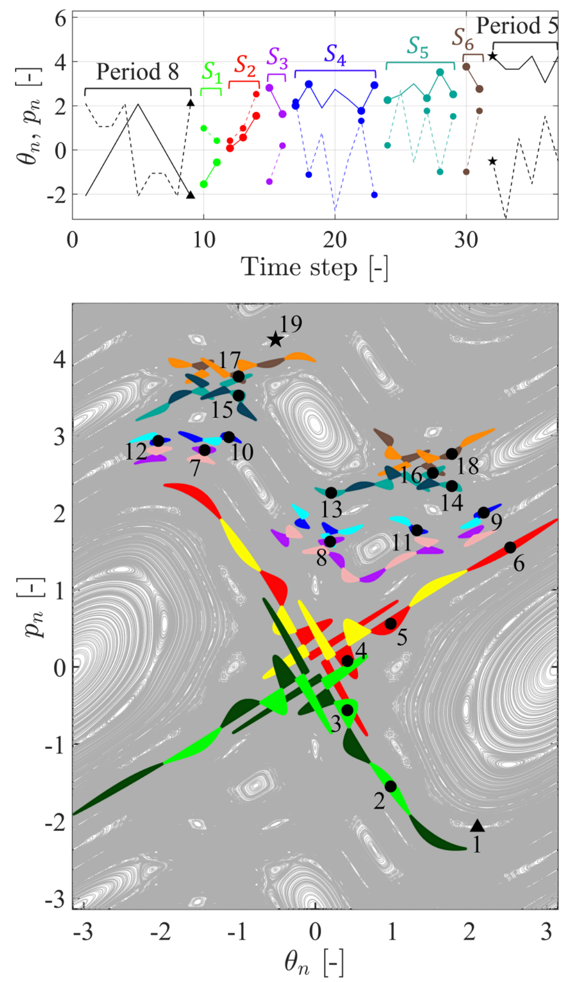


FIG. 3. Optimal trajectory for the standard map with $K = 1.2$, with a total cost $D = 2.1333$ and transfer time $\Delta n = 23$, where $r^* = 0.02$ and $d^* = 0.64$: Controlled time series of $p_n$ (solid line) and $\theta_n$ (dashed line) (top), and state space of the standard map (bottom) are depicted. Gaps on the top panel indicate controlled jumps. Different effective lobe sequences are colored differently. The start point, goal point, and centers of gravity of the adopted lobes are denoted as a triangle, a star, and dots, respectively. The numbers in the bottom panel represent the order of transfer, similar to those in Fig. 2.

framework, each control cost is quantified as $d_n = |\Delta p_n|$, subject to $|\theta'_{n+1} - \theta_{n+1}| < |p'_{n+1} - p_{n+1}| < d^*$. In this example, the start and goal orbits, $O_s$ and $O_g$, are selected as periodic orbits with periods 8 and 5, respectively. All points on each periodic orbit are regarded as potential start/goal points. The minimum lobe radius and maximum jump cost are given as $r^* = 0.02$ and $d^* = 0.64$, respectively. To designate intermediate waypoints, we select 12 effective lobe sequences with up to 9 step lengths. Thus, our scheme finds the optimal trajectory with a total cost $D = 2.1333$ and transfer time $\Delta n = 23$, including the coasting time within lobe sequences without controls, as illustrated in Fig. 3. As a result, our optimal trajectory achieves a short-time transfer. The total cost is larger than the minimum cost of a direct jump from a start point to a goal point ($d_1 = 0.9673$), due to the necessity of multiple jumps under the constraint $d_k < d^* = 0.64$. The colored regions in the lower panel represent the selected 12 effective lobe sequences, from which six effective lobe sequences $S_1, \ldots, S_6$ are adopted, corresponding to colored lines in the upper panel. The gaps in the upper panel signify the controlled jumps.

Similarly, we implement our control scheme for Hill's equation with $J = 3.16$ by utilizing the Poincaré section at perigee passage. The control cost $d_k$ is set as the magnitude of impulsive velocity change at a control point outside the Poincaré section. The controlled jumps in this optimization only change the velocity direction so that the Jacobi integral remains the same. We facilitate a robust transfer originating from one of the periapses of the 7 : 2 neutrally stable resonant orbit and leading to the section at $y = 0$ and $\dot{y} > 0$ within the Moon realm, by focusing on eight effective lobe sequences. The constraint parameters are set as $r^* = 0.002$ and $d^* = 0.097\,60$ [100 (m/s)]. The derived optimal trajectory is illustrated in Fig. 4, and is characterized by a total cost $D = 0.1511$ [154.7849 (m/s)] and transfer time $\Delta t = 37.5827$ [163.2018 (days)], including the coasting time on lobe sequences without control and continuous trajectory outside the Poincaré section until $y = 0$ ($\dot{y} > 0$) around the Moon. The lower panel of Fig. 4 shows the Poincaré section at perigee passage. This Poincaré section is rendered in action $G_d$–angle $g_d$ coordinates by translating the spacecraft's state at a perigee into the canonical variables known as Delaunay elements. An increase in $G_d$ at perigees typically indicates a larger distance between the Earth and spacecraft compared to previous positions. A detailed explanation is given in the Supplemental Material [33]. The region enclosed by the dashed line in the lower panel of Fig. 4 signifies the stable manifold of the Lyapunov orbit, acting as the sole control-free path from the Earth realm to the Moon realm, which corresponds to the goal orbit $O_g$ in our scheme. The colored regions in the lower panel represent the eight selected effective lobe sequences, from which two effective lobe sequences $S_1$ and $S_2$ are adopted, corresponding to colored lines in the upper panel. The transfer time of our optimal trajectory is much shorter than that of the Bollt and Meiss trajectory [748 (days)] [16] and that of the Schroer and Ott trajectory [293 (days)] [17], despite our trajectory starting farther away from the Moon. According to Ref. [2], the cargo transport to the Moon may have a total cost of 0–400 (m/s) and transfer time of several days to 1 year, suggesting that our result of $D = 154.7849$ (m/s) and $\Delta t = 163.2018$ (days) is practically useful for the preliminary trajectory design in the Earth-Moon system.

In summary, we propose a control scheme to design robust trajectories utilizing effective lobe sequences, making the trajectories insensitive to external perturbations. Our scheme reveals that the effective lobes can indicate possible paths to traverse chaotic zones in a short time, with small controls, and with limited fuel. The examples with the standard map and Hill's equation demonstrate that our control scheme can construct trajectories with a short transfer time by leveraging lobe dynamics. In Hamiltonian systems with three or more degrees of freedom, tori may not impede dynamics, which allows the trajectories to migrate from the inside of a torus to the outside. On the other hand, the literature of Refs. [34,35] suggests that stable/unstable manifolds associated with normally hyperbolic invariant manifolds may form lobes in high-dimensional Hamiltonian systems. Thus, the control based on lobes in high-dimensional Hamiltonian systems remains as a challenging future work.

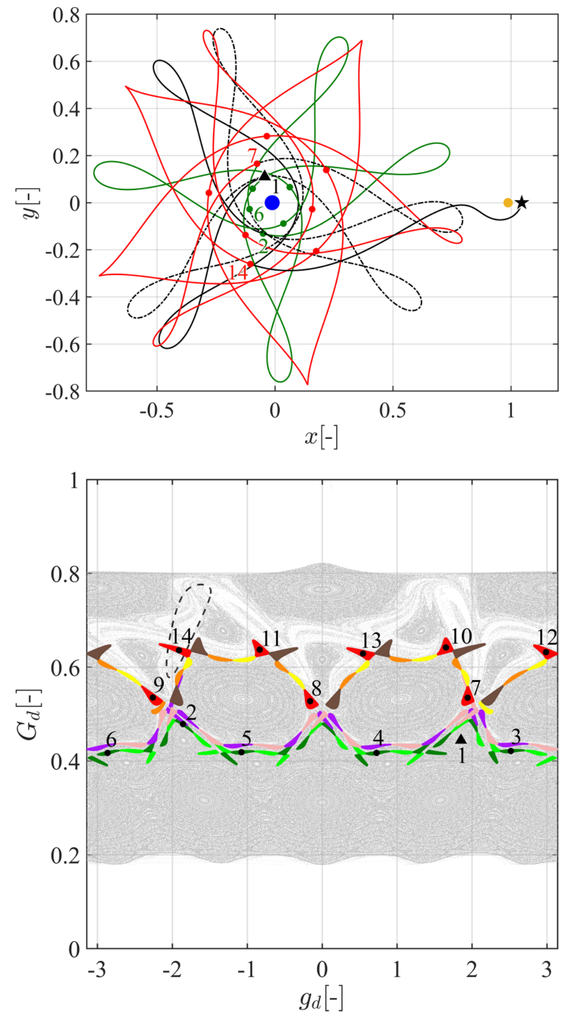


FIG. 4. Optimal trajectory for the Hill's equation with $J = 3.16$, with a total cost $D = 0.1511$ [154.7849 (m/s)] and transfer time $\Delta t = 37.5827$ [163.2018 (days)], where $r^* = 0.002$ and $d^* = 0.097\,60$ [100 (m/s)]: Controlled trajectory in the position space (top) and Poincaré section at perigee passage (bottom) are depicted. A dash-dotted line denotes the controlled transition between effective lobe sequences, and solid lines represent the other part of the transfer. Blue and yellow dots indicate the Earth and Moon, respectively. The region surrounded by a dashed line in the Poincaré section is the gate to the Moon realm. Other notations are the same as those in Fig. 3.

The authors thank Prof. J. D. Meiss and Prof. D. J. Scheeres for their insightful discussions. N.H. acknowledges the support of Japan Society for the Promotion of Science (JSPS) KAKENHI Grant No. JP 23KJ1692. M.B. was supported by Japan Science and Technology Agency (JST) FOREST Program, No. JPMJFR206M, JSPS Grant-in-Aid for Scientific Research (B), JP 22H03663, and JSPS Grant-in-Aid for Challenging Research (Exploratory), JP 21K18781. I.N. thanks the Research Institute for Electronic Science and Department of Mathematics at Hokkaido University for hospitality during his sabbatical leave. Y.S. was supported by JSPS Grant-in-Aid for Scientific Research (B), JP No. 21H01002.

[1] S. Creech, J. Guidi, and D. Elburn, Artemis: An overview of NASA's activities to return humans to the moon, in *2022 IEEE Aerospace Conference (AERO), Big Sky, MT, USA* (IEEE, New York, 2022), pp. 1–7.

[2] T. Ikenaga, K. Yamanaka, S. Ueda, and N. Ishii, Study on the low-energy ballistic lunar transfer orbit for future cargo mission to gateway, in *AIAA Scitech 2020 Forum* (AIAA, Reston, VA, 2020).

[3] S. Bandyopadhyay, R. Foust, G. P. Subramanian, S.-J. Chung, and F. Y. Hadaegh, Review of formation flying and constellation missions using nanosatellites, J. Spacecr. Rockets **53**, 567 (2016).

[4] V. Rom-Kedar and S. Wiggins, Transport in two-dimensional maps, Arch. Ration. Mech. Anal. **109**, 239 (1990).

[5] J. E. Prussing and B. A. Conway, *Orbital Mechanics* (Oxford University Press, Oxford, UK, 1993).

[6] W. S. Koon, M. W. Lo, J. E. Marsden, and S. D. Ross, Heteroclinic connections between periodic orbits and resonance transitions in celestial mechanics, Chaos **10**, 427 (2000).

[7] W. S. Koon, M. W. Lo, and S. D. Ross, *Dynamical Systems, the Three-Body Problem and Space Mission Design* (Marsden Books, 2011).

[8] J. S. Parker and R. L. Anderson, *Low-Energy Lunar Trajectory Design* (Wiley, Hoboken, NJ, 2014).

[9] B. P. McCarthy and K. C. Howell, Four-body cislunar quasi-periodic orbits and their application to ballistic lunar transfer design, Adv. Space Res. **71**, 556 (2023).

[10] S. D. Ross, W. S. Koon, M. W. Lo, and J. E. Marsden, Design of a multi-moon orbiter, Adv. Astronaut. Sci. **114**, 669 (2003).

[11] E. Ott, C. Grebogi, and J. A. Yorke, Controlling chaos, Phys. Rev. Lett. **64**, 1196 (1990).

[12] K. Pyragas, Continuous control of chaos by self-controlling feedback, Phys. Lett. A **170**, 421 (1992).

[13] M. Yamaguti, *Towards the Harnessing of Chaos* (Elsevier, Amsterdam, 1994).

[14] H. Jaeger and H. Haas, Harnessing nonlinearity: Predicting chaotic systems and saving energy in wireless communication, Science **304**, 78 (2004).

[15] T. Shinbrot, E. Ott, C. Grebogi, and J. A. Yorke, Using chaos to direct trajectories to targets, Phys. Rev. Lett. **65**, 3215 (1990).

[16] E. M. Bollt and J. D. Meiss, Targeting chaotic orbits to the moon through recurrence, Phys. Lett. A **204**, 373 (1995).

[17] C. G. Schroer and E. Ott, Targeting in Hamiltonian systems that have mixed regular/chaotic phase spaces, Chaos **7**, 512 (1997).

[18] C. Senatore and S. D. Ross, Fuel-efficient navigation in complex flows, in *Proceedings of the 2008 American Control Conference* (IEEE, New York, 2008), pp. 1244–1248.

[19] A. G. Ramos, V. J. García-Garrido, A. M. Mancho, S. Wiggins, J. Coca, S. Glenn, O. Schofield, J. Kohut, D. Aragon, J. Kerfoot *et al.*, Lagrangian coherent structure assisted path planning for transoceanic autonomous underwater vehicle missions, Sci. Rep. **8**, 4575 (2018).

[20] K. Krishna, Z. Song, and S. L. Brunton, Finite-horizon, energy-efficient trajectories in unsteady flows, Proc. R. Soc. London, Ser. A **478**, 20210255 (2022).

[21] G. Haller, *Transport Barriers and Coherent Structures in Flow Data* (Cambridge University Press, Cambridge, UK, 2023).

[22] J. Duan and S. Wiggins, Lagrangian transport and chaos in the near wake of the flow around an obstacle: A numerical implementation of lobe dynamics, Nonlinear Process. Geophys. **4**, 125 (1997).

[23] C. Coulliette and S. Wiggins, Intergyre transport in a wind-driven, quasigeostrophic double gyre: An application of lobe dynamics, Nonlinear Process. Geophys. **8**, 69 (2001).

[24] F. Lekien, S. C. Shadden, and J. E. Marsden, Lagrangian coherent structures in $n$-dimensional systems, J. Math. Phys. **48**, 065404 (2007).

[25] K. Oshima and T. Yanao, Jumping mechanisms of Trojan asteroids in the planar restricted three- and four-body problems, Celest. Mech. Dyn. Astron. **122**, 53 (2015).

[26] S. Naik, F. Lekien, and S. D. Ross, Computational method for phase space transport with applications to lobe dynamics and rate of escape, Regular Chaotic Dyn. **22**, 272 (2017).

[27] B. V. Chirikov, A universal instability of many-dimensional oscillator systems, Phys. Rep. **52**, 263 (1979).

[28] V. Szebehely, *Theories of Orbits: The Restricted Problem of Three Bodies* (Academic Press, New York, 1967).

[29] V. Rom-Kedar, A. Leonard, and S. Wiggins, An analytical study of transport, mixing and chaos in an unsteady vortical flow, J. Fluid Mech. **214**, 347 (1990).

[30] R. S. MacKay, J. D. Meiss, and I. C. Percival, Resonances in area-preserving maps, Physica D **27**, 1 (1987).

[31] J. D. Meiss, Thirty years of turnstiles and transport, Chaos **25**, 097602 (2015).

[32] R. S. MacKay, J. D. Meiss, and I. C. Percival, Transport in Hamiltonian systems, Physica D **13**, 55 (1984).

[33] See Supplemental Material at http://link.aps.org/supplemental/10.1103/PhysRevResearch.6.L022046 for detailed explanations of the optimization in the standard map and Hill's equation and for the coordinate transformation for the periapsis Poincaré map in Delaunay elements.

[34] S. Wiggins, On the geometry of transport in phase space I. Transport in $k$-degree-of-freedom hamiltonian systems, $2 \leqslant k < \infty$, Physica D **44**, 471 (1990).

[35] M. Dellnitz, O. Junge, W. S. Koon, F. Lekien, M. W. Lo, J. E. Marsden, K. Padberg, R. Preis, S. D. Ross, and B. Thiere, Transport in dynamical astronomy and multibody problems, Int. J. Bifurcation Chaos **15**, 699 (2005).